





## **Chapter 2: Sustaining Star Formation: Gas Conditions & Environment**



# Probing the Conditions for the Atomic-to-Molecular Transition in the Interstellar Medium

Gyueun Park<sup>1,2</sup> , Min-Young Lee<sup>1,2</sup>, Shmuel Bialy<sup>3</sup>,  
Blakesley Burkhart<sup>4,5</sup>, Joanne Dawson<sup>6</sup>, Carl Heiles<sup>7</sup>, Di Li<sup>8,9,10</sup> ,  
Claire Murray<sup>11,12</sup>, Hiep Nguyen<sup>13</sup>, Anita Petzler<sup>6</sup>  
and Snežana Stanimirović<sup>14</sup>

<sup>1</sup>Korea Astronomy & Space Science Institute, 776 Daedeok-daero, Yuseong-gu, Daejeon 34055, Republic of Korea  
email: [gpark@kasi.re.kr](mailto:gpark@kasi.re.kr)

<sup>2</sup>Department of Astronomy & Space Science, University of Science and Technology, 217 Gajeong-ro, Yuseong-gu, Daejeon 34113, Republic of Korea  
email: [mlee@kasi.re.kr](mailto:mlee@kasi.re.kr)

<sup>3</sup>Department of Astronomy, University of Maryland, College Park, MD 20742, USA

<sup>4</sup>Department of Physics and Astronomy, Rutgers University, Piscataway, NJ 08854, USA

<sup>5</sup>Center for Computational Astrophysics, Flatiron Institute, 162 Fifth Avenue, New York, NY 10010, USA

<sup>6</sup>Department of Physics and Astronomy, Macquarie University, NSW 2109, Australia

<sup>7</sup>Department of Astronomy, University of California, Berkeley, CA 94720, USA

<sup>8</sup>National Astronomical Observatories, Chinese Academy of Sciences, Beijing 100101, China

<sup>9</sup>NAOC-UKZN Computational Astrophysics Centre, University of KwaZulu-Natal, Durban 4000, South Africa

<sup>10</sup>Research Center for Intelligent Computing, Zhejiang Laboratory, Hangzhou 311100, China

<sup>11</sup>Space Telescope Science Institute, 3700 San Martin Drive, Baltimore, MD 21218, USA

<sup>12</sup>Department of Physics & Astronomy, Johns Hopkins University, MD 21218, USA

<sup>13</sup>Research School of Astronomy and Astrophysics, The Australian National University, Canberra, ACT 2611, Australia

<sup>14</sup>Department of Astronomy, University of Wisconsin, Madison, WI 53706-15821, USA

**Abstract.** We examine the physical conditions required for the formation of H<sub>2</sub> in the solar neighborhood by comparing H I emission and absorption spectra toward 58 lines of sight at  $b < -5^\circ$  to CO(1–0) and dust data. Our analysis of CO-associated cold and warm neutral medium (CNM and WNM) shows that the formation of CO-traced molecular gas is favored in regions with high column densities where the CNM becomes colder and more abundant. In addition, our comparison to the one-dimensional steady-state H I-to-H<sub>2</sub> transition model of Bialy et al. (2016) suggests that only a small fraction of the clumpy CNM participates in the formation of CO-traced molecular gas. Another possible interpretation would be that missing physical and chemical processes in the model could play an important role in H<sub>2</sub> formation.

**Keywords.** ISM: atoms – ISM: clouds – dust, extinction – ISM: molecules – ISM: structure – radio lines: ISM

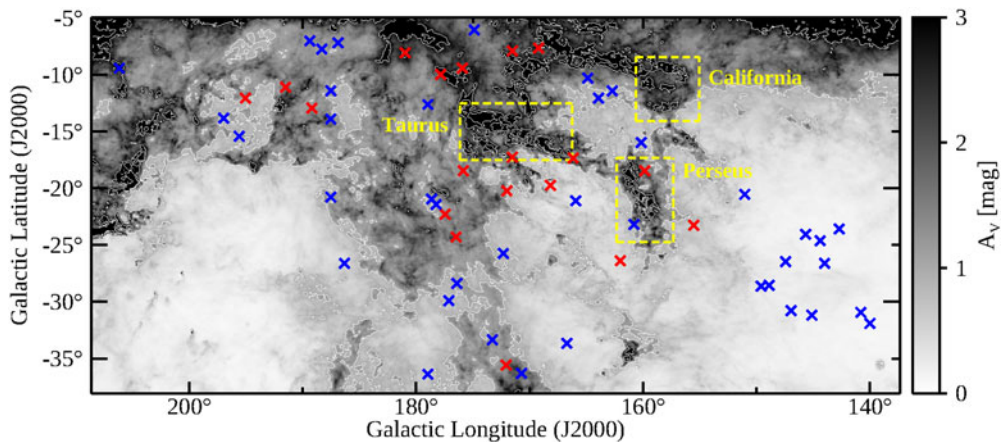


**Figure 1.** Our 58 LOSs are marked on the *Planck*  $A_V$  map at  $b < -5^\circ$  (Planck Collaboration *et al.* 2016) with contours 1, 3, and 5 mag in white. The 19 LOSs marked in red crosses show clear CO(1–0) detection, while the remaining 39 LOSs marked in blue crosses show no CO(1–0) detection. The yellow boxes represent the approximate locations of local molecular clouds (Perseus, Taurus, and California).

## 1. Introduction

Molecular clouds, the principal stellar nurseries, form out of the surrounding diffuse gas through the conversion of atomic (H I) to molecular hydrogen ( $H_2$ ). Among the two main flavors of H I (cold and warm neutral medium; CNM and WNM), the colder and denser CNM (spin temperature  $T_s \simeq 60\text{--}260$  K; gas density  $n \simeq 7\text{--}70$   $\text{cm}^{-3}$ ) is expected to be more critical for the conversion, and yet its exact roles remain largely unknown due to a difficulty in direct measurements.

To overcome observational challenges and provide unique insights into the roles of the CNM in the formation of molecular gas, we obtained Arecibo H I emission and absorption spectra (angular and velocity resolution of  $3.5'$  and  $0.16$   $\text{km s}^{-1}$ , respectively) toward 58 lines of sight (LOSs) at  $b < -5^\circ$  (Figure 1; Stanimirović *et al.* 2014; Nguyen *et al.* 2019) and analyzed them with TRAO/PMO CO(1–0) emission spectra (angular and velocity resolution of  $48''$  and  $0.32$   $\text{km s}^{-1}$ , respectively). For 19 CO-detected LOSs where we have optical depth ( $\tau_{\text{CNM}}$ ), spin temperature ( $T_s$ ), and column density ( $N_{\text{CNM}}$  and  $N_{\text{WNM}}$ ) estimates, the CO spectra were fitted and decomposed into individual Gaussians to derive line parameters such as the central velocity ( $\nu_{\text{CO}}$ ) and line width (FWHM;  $\Delta\nu_{\text{CO}}$ ).

In this article, we present our study on the H I-to- $H_2$  transition from two perspectives: observational (comparison between H I and CO) and theoretical (comparison between our observations and the analytic model of Bialy & Sternberg 2016 (B16 hereafter)) approaches.

## 2. Conditions for the Formation of Molecular Gas: Observational Perspective

### 2.1. Kinematic Association between H I and CO

To investigate the H I conditions that are favorable to form molecular gas, we first compared the central velocities of H I and CO. In Figure 2, we included H I components that are closest to CO emission in velocity and displayed the absolute velocity differences between H I and CO in cumulative distribution function (CDF).

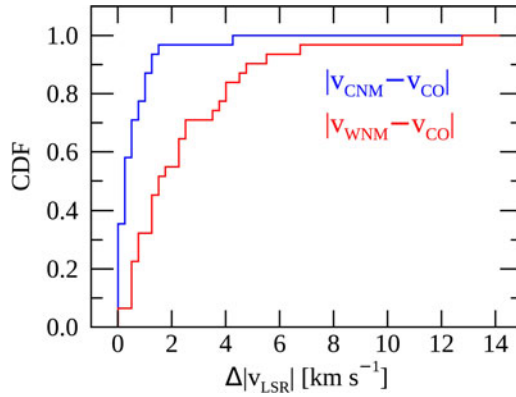


**Figure 2.** CDF of the absolute velocity difference between H I and CO (blue:  $|\nu_{\text{CNM}} - \nu_{\text{CO}}|$ ; red:  $|\nu_{\text{WNM}} - \nu_{\text{CO}}|$ ). For this plot, only the CNM and WNM components that are closest to the observed CO emission in velocity are considered.

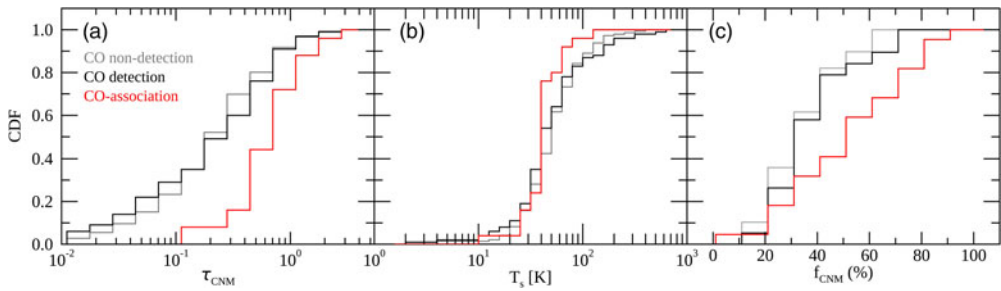


**Figure 3.** CDFs of (a) optical depth, (b) spin temperature, and (c) CNM fraction. In each panel, the three groups are shown in different colors (gray: CO non-detection; black: CO detection; red: CO-association).

As shown in Figure 2, the velocity difference between CNM-CO has a range of 0.01–4.3 km s<sup>-1</sup> with a median of 0.4 km s<sup>-1</sup>, while that of WNM-CO ranges from 0.03 km s<sup>-1</sup> to 12.8 km s<sup>-1</sup> with a median of 1.9 km s<sup>-1</sup>. The systematically smaller velocity difference between the CNM and CO suggests that the CNM is kinematically more closely associated with CO emission. If velocity is taken as a proxy for distance, our result implies that the CO-traced molecular gas forms in CNM environments.

## 2.2. H I Properties

Next, we investigated the properties of CO-associated CNM components by classifying the observed CNM into three groups: (1) CO non-detection (all components toward the 39 CO not-detected LOSs); (2) CO detection (all components toward the 19 CO-detected LOSs); (3) CO-association (components whose central velocities are within  $\nu_{\text{CO}} \pm \Delta\nu_{\text{CO}}$ ). We note that the CO-association is a subset of the CO detection.

For each group, we show the distributions of the individual optical depth ( $\tau_{\text{CNM}}$ ) and spin temperature ( $T_s$ ), as well as the integrated CNM fraction (CNM-to-total H I column density ratio;  $f_{\text{CNM}}$ ), in Figure 3. Generally, the CO non-detection and detection groups are comparable in terms of the CNM properties. On the contrary, the CO-association has several distinctive features compared to the CO non-detection and detection groups. For example, its minimum  $\tau_{\text{CNM}} \sim 0.1$  and maximum  $T_s \sim 130$  K are larger and smaller by

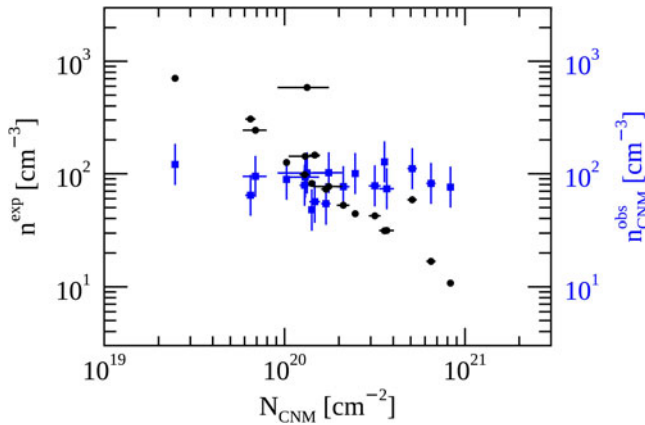


**Figure 4.** Comparison between the B16-based total densities (circles in black) and the observationally inferred CNM densities (squares in blue) as a function of the CNM column density. For this plot, the 19 CO-detected LOSs are included. As B16 predicts total densities expected for H<sub>2</sub> formation,  $n_{\text{CNM}}^{\text{obs}}$  should be lower than  $n^{\text{exp}}$ . The variation in the assumed thermal pressure ( $\log_{10}(P/k_B) = 3.58 \pm 0.18 \text{ K cm}^{-3}$ ) is indicated as the  $1\sigma$  error bars for  $n_{\text{CNM}}^{\text{obs}}$ .

a factor of ten and five, respectively, than those for the other two groups. Moreover, its median  $f_{\text{CNM}} \sim 0.6$  is 1.5 times larger than that of the CO non-detection and detection groups. Overall, our result implies that the formation of CO-traced molecular gas is favored in environments where the CNM becomes colder and more abundant.

### 3. Conditions for the Formation of Molecular Gas: Theoretical Perspective

#### 3.1. Density versus CNM column density

With the aim of probing the underlying principles of the H I-to-H<sub>2</sub> transition, we compared the observed CNM properties to the B16 model. B16 predicted the total H I column density in a one-dimensional slab of gas and dust irradiated by isotropic UV radiation as a function of UV radiation field strength ( $I_{\text{UV}}$ ), dust absorption cross-section ( $\tilde{\sigma}_g$ ), and total hydrogen density ( $n = n(\text{H I}) + n(\text{H}_2)$ ) by assuming H<sub>2</sub> formation in steady-state and chemical equilibrium. Given that our LOSs probe solar neighborhood environments ( $\tilde{\sigma}_g \sim 1$ ), the total H I column density can simply be expressed as a function of  $I_{\text{UV}}$  and  $n$ :

$$N(\text{H I}) = 8.4 \times 10^{20} \ln \left( \frac{18.4 I_{\text{UV}}}{n} + 1 \right) \text{ (cm}^{-2}\text{)}. \quad (1)$$

Using our observed CNM column density ( $N_{\text{CNM}}$ ) and spin temperature ( $T_s$ ) and assuming the measured thermal pressure of  $\log_{10}(P/k_B) = 3.58 \pm 0.18$  from Jenkins & Tripp (2011), we can make a comparison between the observationally inferred CNM density:

$$n_{\text{CNM}}^{\text{obs}} = \left( \frac{10^{3.58 \pm 0.18}}{T_s} \right) \text{ (cm}^{-3}\text{)}, \quad (2)$$

and the theoretically expected total density:

$$n^{\text{exp}} = \frac{18.4 I_{\text{UV}}}{\exp(N_{\text{CNM}}/8.4 \times 10^{20}) - 1} \text{ (cm}^{-3}\text{)}, \quad (3)$$

where *Planck*-based  $I_{\text{UV}}$  estimates in units of the Draine field (Planck Collaboration et al. 2016) are:

$$I_{\text{UV}} = \left( \frac{T_{\text{dust}}}{17.5 \text{ K}} \right)^{\beta+4}. \quad (4)$$

For Equation 1, we substituted  $N(\text{H I})$  into  $N_{\text{CNM}}$ . This is based on the fact that the observed uniform  $I_{\text{UV}} \sim 1$  likely represents isotropic UV radiation attenuated by the widespread WNM: the impact of the WNM on the H I-to- $\text{H}_2$  transition is hence already considered. As B16 predicts total densities expected for  $\text{H}_2$  formation, the CNM density ( $n_{\text{CNM}}^{\text{obs}}$ ) should be a lower limit on the total gas density ( $n^{\text{exp}}$ ).

Since the real structure of gas is unknown, we assumed that only the CNM close to CO (within  $\nu_{\text{CO}} \pm \Delta\nu_{\text{CO}}$ ; CO-association) is highly effective in shielding molecular gas from dissociating UV photons. This assumption of conservative geometry would be the case of a small volume filling factor, making the penetration of UV radiation into the CNM easier.

Figure 4 shows that the predicted total densities are consistent with the lower limits provided by our measurements at low column densities ( $N_{\text{CNM}} \lesssim 10^{20} \text{ cm}^{-2}$ ). On the other hand, the observationally inferred CNM densities are higher than the B16-based total densities at high column densities ( $N_{\text{CNM}} \gtrsim 10^{21} \text{ cm}^{-2}$ ), resulting in by up to an order of magnitude discrepancy.

### 3.2. Limitations and Implications of B16

The discrepancy between our observations and the B16 model at high CNM column densities indicates that only a small fraction of the CNM along a LOS ( $\lesssim 30\%$  on average; estimated from the LOSs at  $N_{\text{CNM}} > 10^{20} \text{ cm}^{-2}$  for the CO-association) contribute to  $\text{H}_2$  formation. In other words, the distribution of the CNM should be clumpy with a small volume filling factor.

While the above interpretation is certainly viable, our analysis may have some limitations. For example, one possible source of the discrepancy is the assumed thermal pressure of  $2500\text{--}5800 \text{ K cm}^{-3}$  for the CNM. Recently, Goldsmith et al. (2018) found a larger variation in  $P/k_{\text{B}}$  ( $\sim 10^3\text{--}10^4 \text{ K cm}^{-3}$ ) in the ISM. If  $P/k_{\text{B}}$  of the CNM varies by an order of magnitude as Goldsmith et al. (2018) suggested, the discrepancy between our observations and the B16 model would decrease. Yet, the discrepancy would still exist at  $N_{\text{CNM}} \gtrsim 10^{21} \text{ cm}^{-2}$ .

Another possible source of the discrepancy is physical and chemical processes that are not considered in the simple steady-state  $\text{H}_2$  formation model of B16, e.g., cosmic-rays and turbulence. These missing ingredients could play an important role in the H I-to- $\text{H}_2$  transition and need further studies.

## 4. Summary

We performed TRAO/PMO CO(1–0) observations toward 58 LOSs at  $b < -5^\circ$  where we have Arecibo H I absorption and emission spectra. For 19 out of the 58 LOSs with clear CO detection, we compared the H I and CO spectra and analyzed the CNM properties to constrain the physical conditions for the H I-to- $\text{H}_2$  transition in the solar neighborhood. Our primary results are as follows:

- (1) The CNM is kinematically (spatially if velocity is considered as a proxy for distance) more closely associated with CO than the WNM.
- (2) The formation of CO-traced molecular gas is favored in environments where the CNM becomes colder and more abundant.

- (3) The comparison with the B16 model suggests that the distribution of the CNM should be clumpy with a small volume filling factor, and only a small fraction of the total CNM along a LOS contributes to H<sub>2</sub> formation. Another possibility is that missing processes in the model, such as cosmic-rays and turbulence, play an important role in the H I-to-H<sub>2</sub> transition.

## References

- Bialy, S. & Sternberg, A. 2016, *ApJ*, 822, 83  
Goldsmith, P. F., Pineda, J. L., Neufeld, D. A., *et al.*, 2018, *ApJ*, 856, 96  
Jenkins, E. B. & Tripp, T. M. 2011, *ApJ*, 734, 65  
Nguyen, H., Dawson, J. R., Lee, M.-Y., *et al.*, 2019, *ApJ*, 880, 141  
Planck Collaboration, Aghanim, N., Ashdown, M., *et al.*, 2016, *A&A*, 596, A109  
Stanimirović, S., Murray, C. E., Lee, M.-Y., *et al.*, 2014, *ApJ*, 793, 132